BOGDAN SZYBIŃSKI *, *ANDRZEJ TROJNACKI* *

ANALYTICAL AND NUMERICAL SOLUTIONS OF METAL HIGH-PRESSURE WAVE-RING GASKET AND COMPARISON WITH EXPERIMENTAL RESULTS

The paper deals with experimental investigations of a set of metal wave-ring gaskets of different thickness and different assembly interference. The gaskets were examined under assembly conditions, i.e. pressed in their seats with no operating pressure applied. The electric resistance wire strain gauges were used to measure the circumferential and axial strains at the inner surface of the gaskets. The traces of contact at the working surface of the gaskets were measured after disassembly the gaskets from their seats. The material tests were carried out to determine the real mechanical properties of materials applied for the gaskets and the seats. The results of experiment were verified by FEM calculations and compared with the analytical approach based on the simplified shell model proposed for the gasket.

Notation

B	–	Bielaev point
c_1 to c_4	–	trigonometric functions of the parameter β
C_1, C_2	–	constants of integration
e	–	width of the contact region
E, ν	–	Young's modulus and Poisson's ratio
E_{t1}, E_{t2}	–	tangent moduli of the stress-strain curve
$2h$	–	distance between the centers of radii R_1
K	–	bending stiffness of the gasket model
$2l$	–	width of the gasket

* *Institute of Machine Design, Cracow University of Technology, Al. Jana Pawła II No. 37, 31-864 Kraków, Poland; E-mail: boszyb@mech.pk.edu.pl; atroj@mech.pk.edu.pl*

M_φ, M_x, N_φ	–	cross-sectional moments and forces
n	–	relation between q_{max} and $R_{0.2}$
n_B	–	relation between σ_{Beq} and $R_{0.2}$
p	–	operating pressure
q	–	initial contact pressure
$q_{m\,opr}$	–	average operating contact pressure
$q_{max\,opr}$	–	maximum operating contact pressure due to the Hertz distribution
Q_x	–	shear force at the support
r	–	mean radius of the gasket model
$R_{0.2\,g}$	–	yield limit of the gasket material
R_1	–	radius of curvature of the gasket working surface
t	–	mean thickness of the gasket model
w	–	deflection of the gasket model
w_h	–	radial displacement of the seat
z, φ, x	–	cylindrical coordinates
Z	–	position of the Bielaev point
β	–	parameter
δ	–	relative error of FEM approximation
Δ	–	initial interference
ε_{eq}	–	equivalent strain
ε'_s, S_c	–	parameters of the approximation of the stress-strain curve
ε_z, ε_φ, ε_x	–	components of strain
$(\varepsilon_{0.05}$, $R_{0.05})$, $(\varepsilon_{0.2}$, $R_{0.2})$, (ε_{max}, R_m)	–	coordinates of the material proportional limit, yield stress and maximum tensile stress, respectively
$\emptyset A$, $\emptyset B$, $\emptyset C$	–	diameters of the gasket
κ, κ_1, κ_2	–	thickness ratios
μ	–	friction coefficient
σ_{Beq}	–	equivalent Bielaev stress
σ_{eq}	–	equivalent stress
σ_z, σ_φ, σ_x	–	components of stress

Subscripts

el	–	elastic
eq	–	equivalent
max	–	maximum
min	–	minimum
nom	–	nominal
pl	–	plastic

1. Introduction

High technical requirements of advanced chemical technologies (pressure, temperature), application of corrosion-resistant materials (high quality alloy steels) and additional brief foredesigns (e.g. possibility of convenient uncoupling of the gasketed members) cause serious difficulties with leak tightness of chemical equipment. In such cases, the wave-ring gasket is often used to seal the heads of pressure vessels and temporary pipe connections, in particular these of greater diameter.

Temporary closures with self-sealing wave-ring gaskets were developed by Imperial Chemical Industries in England more than 70 year ago [1]. Unfortunately, in opposite to another types of joints (e.g. flanged pipe joints) wave-ring gaskets are not adequately presented in technical literature. Moreover, no procedures exist which can be applied in design calculations of the gaskets. Actually, dimensions of wave-ring gaskets, their material and the initial interference fit vary quite widely and depend in general on the applied pressure, although the joints function properly [2].

The presented paper follows earlier theoretical investigations of the authors [3-6] devoted to the wave-ring gaskets and presented in [7] estimation of several analytical models of the gasket verified by FEM modeling. The aim of the paper is the experimental verification of a certain simple computational model of the wave-ring gasket which could be applied to develop engineering formulae and codes to determine geometry, material properties, assembly requirements and working parameters of wave-ring gaskets.

2. Engineering example and service conditions of the sealing

The wave-ring gasket is a certain type of self-sealing gaskets for very high pressure chemical equipment. Engineering example of the joint with wave-ring gasket between the vessel wall and the reactor head is shown in Fig. 1. The geometry of the gasket is presented in detail A in Fig. 1. The

closure is successfully applied [2] in the heavy-duty chemical equipment working at the pressure of 200 MPa.
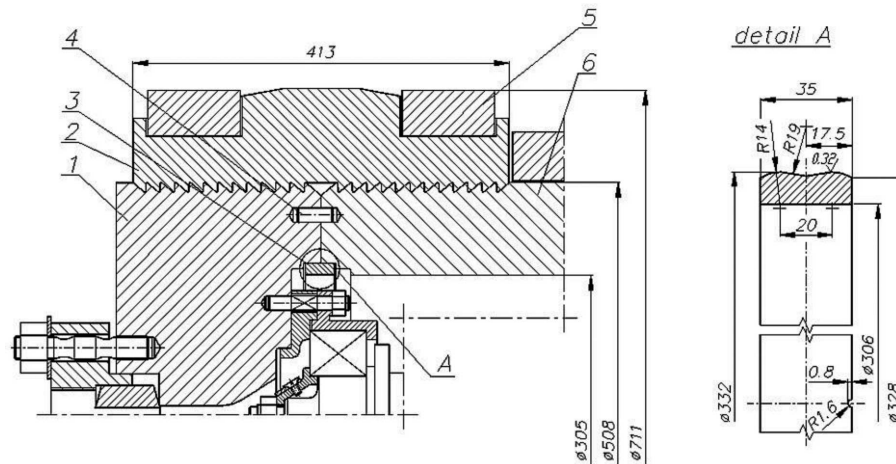

Fig. 1. Engineering example of the joint between the vessel wall and the reactor head: 1 – head, 2 – sectional clamping rings, 3 – wave-ring gasket, 4 – locating pin, 5 – grips, 6 – cylindrical shell. Detail A – geometry of the wave-ring gasket

The yield stress of the wave-ring gasket material must be significantly lower than the yield stress of the seat material to ensure the proper effectiveness of the joint. The gasket is usually made of low-carbon soft steel subjected to the heat refining to the yield limit of approximately 400 MPa. Sometimes the gasket is fabricated of copper, brass, or some other moderately soft metal. The high-quality chromium-nickel-molybdenum steel hardened to the yield limit of minimum 750 MPa is mostly used for the seats. The gasket must be made slightly oversized, so that an interference fit is obtained in the seat. The experience gathered with existing and properly running closures leads to the conclusion that the degree of the preferred radial interference between the external wave surface of the gasket and the cylindrical internal surface of the seat may vary from 0.5‰ to 2.0‰ and depends on the yield limit of the gasket material and on the operating pressure.

Under assembly conditions, the initial contact pressure q appears at the portion e of a wave surface due to the assembly interference, thus making the initial seal just before the operating pressure p is applied to the closure (Fig. 2). The working pressure is exerted on the entire inner surface, forcing a seal on the two outer radii. The initial assembly pressure q increases as the stiffness of the gasket is much less than that of the seat. Because of its specific features such a sealing may be applied in equipment working at extremely high pressure, much more than 100 MPa.
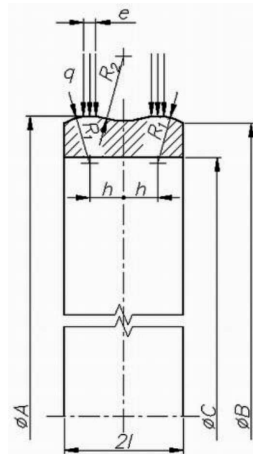
Fig. 2. Distribution of initial load at the contact region of the gasket

The difference in the yield limits of materials of the gasketed members and the value of the radial interference fit are the key parameters of the closure. They have an essential influence on the width of the contact zone of required size and on the related contact pressure value which provide the leak tightness of the connection under the operating pressure p. In the simple preliminary calculations of practical engineering applications of the wave-ring gaskets the non-leakage condition is usually formulated as

$$q_{m\,opr} > R_{0.2\,g} \geq 2p, \tag{1}$$

where $q_{m\,opr} = 2q_{\max\,opr}/3$ as for the parabolic elastic distribution due to the Hertz theory. Because of highly approximate estimation of the contact stress distribution, the average value of the distribution is introduced into equation (1). It means that the average contact pressure $q_{m\,opr}$ in the contact zone under operating conditions must be greater than the yield limit $R_{0.2\,g}$ of the gasket and should at least twice exceed the operating pressure p. The magnitude of the yield limit of the gasket material and the size of the radial interference fit are related and depend strongly on the applied operating pressure. The influence of several parameters of the connection on its sealing properties in the operating conditions was investigated in dimensionless variables in [6]. The dimensionless non-leakage parameter was defined as $\psi = q_{m\,opr}/2p$ and the simplified analytical approach was applied to obtain the solution. The present paper deals with the sealing in the gaskets installation conditions, where the connection is not subjected to the external operating loading. In this case, the development of the contact region width and changes in related contact pressure being the crucial sealing parameters are not analysed.

Wave-ring gaskets give satisfactory service where the vessel or piping need not to be opened very often. In the opposite case they are somewhat

impractical, as they sometimes become so tightly wedged that the vessel head can be removed only with extreme difficulty. When this jamming occurs, the gasket usually must be discarded, as the crests have been flattened and scarred. Where the closure must be opened and closed fairly often, the gasket is sometimes made of hardened steel.

In conclusion, it should be noted that there is no design objectives and constraints which are collected and can be recommended in the design procedures of the closures with wave-ring gaskets. The parameters of the new connections are selected basing on the experience gained during operating and improving of the existing sealing systems. Moreover, in each individual case of technical application a set of expensive and time-consuming calculations and experimental tests should be carried out to confirm the accuracy of the choice as the sudden decrease of the leak tightness of the very high-pressure installation may cause serious damages.

3. The test stand

The construction of the test stand is shown in Fig. 3. The examined wave-ring gasket 3 is located inside two sectional seats 4 which are placed into external holders 2 and 6 and put on the footing 1. The holders are provided with two locating pins 8 to ensure alignment of the seats and the holders during the mounting operation. The guard fingers 7 are applied to fix the position of the gasket with respect to both segments 4 of the seat. The screws 5 are used to disassembly the gasket and the seats after the experiment.

Six sets of wave-ring gaskets and corresponding sectional seats were tested in the experiment under assembly conditions (in the gaskets installation state). The gaskets were made of the forged bar of soft 25CrMo4 (1.7218) – EN 10083-4 chromium-molybdenum normalized steel using machining. The ultrasonic method was applied to check the quality (the cracks) of the semi-finished steel. The seats were made of 42CrMo4 (1.7225) high-carbon chromium-molybdenum steel toughened to $R_m = 900 \div 1000$ MPa, and 41Cr4 (1.7035) chromium steel was used for the holders and the footing. The mechanical properties of 25CrMo4 and 42CrMo4 steels were verified experimentally. Two cylindrical specimens were subjected to the same heat treatment as the corresponding elements, and prepared for the static tensile tests. The obtained real load-displacement curves $F = f(\Delta l)$ are shown in Fig. 4. The strength properties of both materials, calculated as arithmetic means of the two tests, are given in Table 1. Experimentally-verified Brinell hardness number of the sealing surfaces of the gaskets was of 250-280 BHN and Rockwell hardness number of the seats was of 45-48.
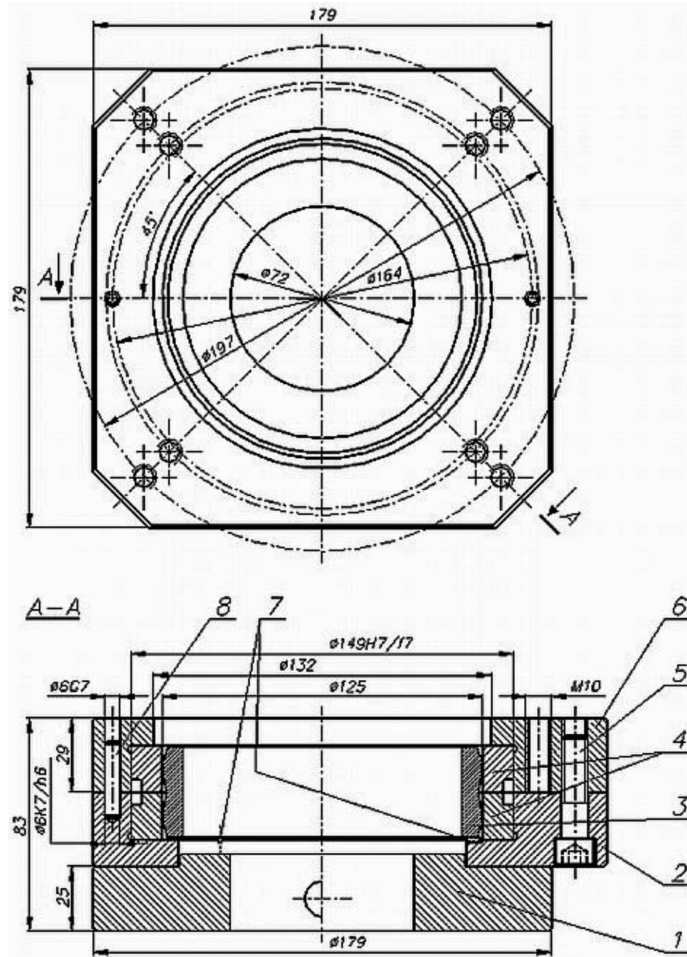
Fig. 3. Test stand: 1 – footing, 2 – lower external holder, 3 – examined wave-ring gasket, 4 – sectional seats, 5 – disassembly screw, 6 – upper external holder, 7 – guard fingers, 8 – locating pin

Table 1.

Strength properties of materials applied for the gaskets and the seats

	Steel	E [MPa]	$R_{0.05}$ [MPa]	$R_{0.2}$ [MPa]	R_m [MPa]	$\varepsilon_{0.05}$ [%]	$\varepsilon_{0.2}$ [%]	ε_{max} [%]
Gasket	25CrMo4(N)	2.014×10^5	253.59	260.30	523.38	0.185	0.359	15.338
Seat	42CrMo4(T)	2.064×10^5	809.12	812.46	918.50	0.460	0.711	8.802

The practically confirmed geometry of the closure [2] was adopted to design the dimensions of the gaskets, in particular with respect to the outer working surface (Fig. 1, detail A). All the gaskets were designed with the same nominal outer diameter $ØA = 125$ mm, the same width $2l = 35$ mm
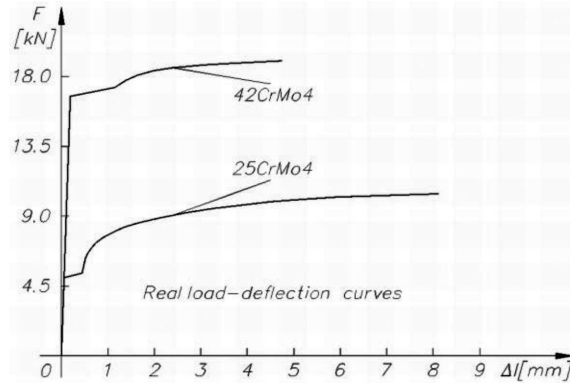
Fig. 4. Results of the static tensile tests of 25CrMo4 (N) and 42CrMo4 (T) materials – real load-displacement curves $F = f(\Delta l)$

and identical geometry of the external working wave surface described by the radius $R_1 = 14$ mm and the distance $2h = 20$ mm between the centers of both radii R_1. The only difference between the gaskets was in the inner diameter: three gaskets were designed with $\varnothing C = 109$ mm and three others with $\varnothing C = 105$ mm (Fig. 5).
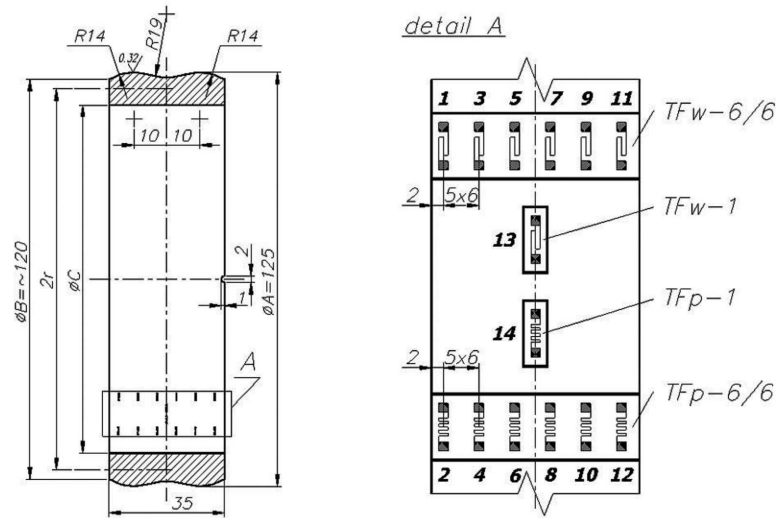

Fig. 5. Geometry of the gaskets. Detail A – localization of the gauges

The gaskets and sectional seats were compiled into two groups. The gaskets in each group had the same thickness but different nominal radial interference Δ_{nom} in the seats. Three values of initial relative assembly interference were accepted in each group, namely 0.48‰, 0.96‰ and 2.0‰. Inner and outer diameters $\varnothing C$ and $\varnothing A$ of the gaskets, inner diameters of the seats and resultant dimensional interferences with respect to the radius

are collected in Table 2 for all six sets of the gaskets and the seats. The dimensions were executed with specified tolerances, so the real interference Δ is unknown. In each case, minimum Δ_{min} and maximum Δ_{max} interferences are presented together with the nominal interference Δ_{nom}.

<div align="right">Table 2.</div>

<div align="center">Dimensions of the gaskets and the seats and applied interferences</div>

No. group	Gasket diameter $\emptyset C$ [mm]	No. set	Gasket diameter $\emptyset A$ [mm]	Seat diameter [mm]	Relative interference [‰]	Radial interference		
						Δ_{min} [mm]	Δ_{nom} [mm]	Δ_{max} [mm]
1	109	A	125.05 $^{\pm0.01}$	124.99 $^{\pm0.01}$	0.48	0.020	0.030	0.040
		B	125.08 $^{\pm0.01}$	124.96 $^{\pm0.01}$	0.96	0.050	0.060	0.070
		C	125.05 $^{\pm0.01}$	124.80 $^{\pm0.01}$	2.00	0.115	0.125	0.135
2	105	A	125.02 $^{\pm0.01}$	124.96 $^{\pm0.01}$	0.48	0.020	0.030	0.040
		B	125.05 $^{\pm0.01}$	124.93 $^{\pm0.01}$	0.96	0.050	0.060	0.070
		C	125.12 $^{\pm0.01}$	124.87 $^{\pm0.01}$	2.00	0.115	0.125	0.135

The strains were measured with electric resistance wire strain foil gauges. Two strips with 6 gauges were placed at the inner cylindrical surface of each gasket: one strip with gauges set in circumferential direction and one strip with gauges set in axial direction. Additionally, two single gauges: one circumferential and one axial were located in the central surface. The gauge strips and single gauges were located as shown in Fig. 5, detail A. The axis of the gauge strips and single gauges were shifted in the circumferential direction with respect to each other at an angle $\pi/3$. The gauges were connected with the static digital resistance bridge through multi-channel switch chests. The gaskets were forced into the seats by means of a hydraulic press with the control of the pressure force.

The test stand prepared for the experiment is shown in Fig. 6a and a detail of the gasket showing the gauges is presented in Fig. 6b.

4. Numerical calculations (FEM)

The results of experiment were obtained in the gasket installation conditions. For this reason, the numerical calculations refer to the assembly conditions in which the loading of the joint is caused by the interference fit only.

The investigated structure is composed of three parts: two outer sectional seats and the wave-ring gasket placed inside the seats. These parts are assembled with an interference fit existing between the external wavy surface of the gasket and the inner cylindrical surface of both seats. The shape of the
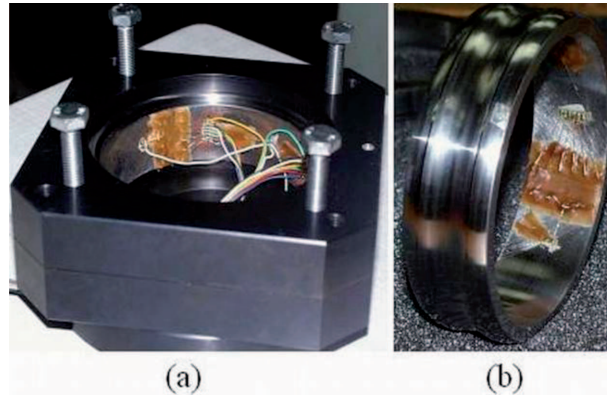
Fig. 6. (a) – test stand prepared for the experiment; (b) – detail of the gasket showing the strain gauges

structure and relatively high radial interference, which should preserve the leak tightness of the junction under operating pressure, result in high stresses and stress gradients distributed over the small zones in the vicinity of contact areas. The problem considered in the paper concerns the contact of two deformable bodies and belongs to the class of flexible-to-flexible contact, for which the analytical solutions are known only in a limited number of simple cases. The contact tasks are nowadays solved numerically, by means of the finite element approximation. This approach additionally enables the analysis of such contact problems, in which the plastic deformations are expected. In the present paper, the ANSYS$^{\circledR}$ code [8] was used to solve the problem and to get the strain and stress distributions in all contacting bodies. Also the contact pressure distribution and the range of the contact zone were the results of that analysis.

In the case of contact of deformable bodies, which are assembled with certain interference, it is recommended to use the so-called surface-to-surface contact elements. Such elements can be of higher order approximation with inside nodes introduced. This provides better results for many engineering applications and enables modeling complex, curved shapes of bodies being in touch. The above contact elements are defined on the surface geometry and need several constants and options to set prior to the analysis. In the investigated problem, the augmented Lagrangian method was used with contact detection points localized in nodal points. Also, the contact stiffness update in each iteration step based on the current mean stress was applied. The Coulomb friction law was used in the analysis.

In general, the analysed structure should be modeled as a 3D object, which results in a very big numerical model and demands a lot of time to get the solution. The size of the task can be reduced when the ideal

geometry of the junction is presumed. Then, the structure is assumed to be axially-symmetric and only the half-part of the cross-section is considered. The high accuracy of numerical results was provided by application of the 8-node quadrilateral axisymmetrical finite elements, which are well-suited for irregular meshes and tasks with elastic and plastic deformations. These elements are accompanied with the contact elements introduced on lines where the contact is expected. Like in the majority of nonlinear problems, the number of applied finite elements should be rather high and the dense meshes should be used in order to keep the solution error within the acceptable range, in particular in the vicinity of the contact zones. The mesh in this area should be dense enough to give satisfying results, while the mesh on the outer unloaded surfaces can be rather rough [9].

In the first numerical approach (FEM 1), the interferences between the gasket and both sectional seats were arranged by means of the thermal method. For the calculation purpose, the gasket was first cooled down and after inserting into the seats and expanding the appropriate interference fits were obtained in the closure. The thermal simulation of the assembly process leads to the same (symmetric) results in displacements, stresses and contact pressure in both half-parts of the axial cross-section.

The second numerical approach (FEM 2) follows the assembly process performed on the stand during the experiment. The nonlinear contact analysis was divided into two steps. In the first step, the gasket was pressed into the bottom sectional seat (supported vertically), while in the second one the upper seat was pressed down until the edges of both seats have got in touch. In the second step the bottom edge of the bottom seat and the bottom edge of the gasket were blocked against the vertical displacement. In this case, the symmetry of results with respect to the middle surface disappears.

Even with the introduced simplifying assumptions and restrictions concerning the geometry and loading (axial symmetry), the numerical solution is time consuming and difficult to obtain due to the numerical instability. The size of the finite elements in the anticipated contact zone and the size of the load step should be chosen with the particular care in order to avoid the convergence problems. Several numerical trials have been carried out to get the final mesh, which is shown in Fig. 7. As a final criterion for the choice of the element size in the contact area, the compromise between the calculation time and the approximation error has been established. The criterion used for the approximation error δ is based on the comparison between the maximum absolute value of the radial stress $\sigma_{z\,max}$ and the maximum contact pressure q_{max} and accepts the mesh for which the discrepancy is less than 5% for each load step [10, 11]

$$\delta = \frac{\|\sigma_{z\,\max}\| - q_{\max}\|}{q_{\max}} 100\% \leq 5\%. \tag{2}$$
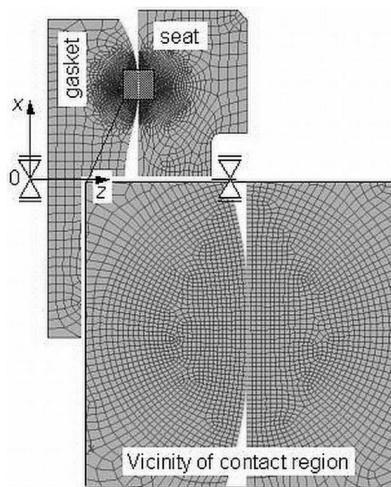

Fig. 7. Example of the mesh of finite elements, division of the closure into parts and illustration of the boundary conditions

The exemplary distribution of the contact pressure q in the closure is depicted in Fig. 8 for the set 2A and the minimum interference. The numerical results are obtained applying FEM 2 procedure for the upper part of the wave-ring gasket which is assembled in the second step.
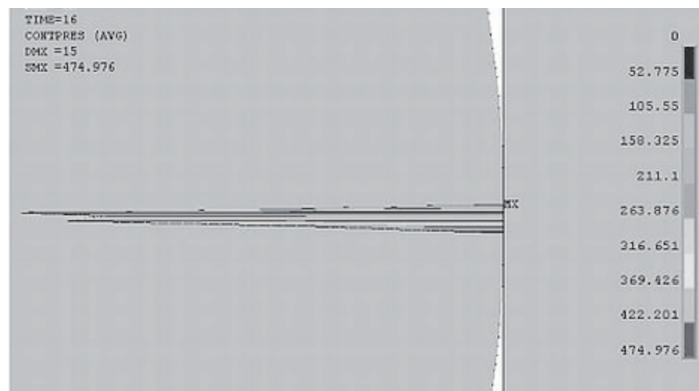

Fig. 8. The exemplary distribution of the contact pressure q in the closure for the set 2A and the minimum interference

Two approximations of the real stress-strain curves $\sigma = f(\varepsilon)$ of the materials used for the gasket and the seat were adopted in the paper. The parameters
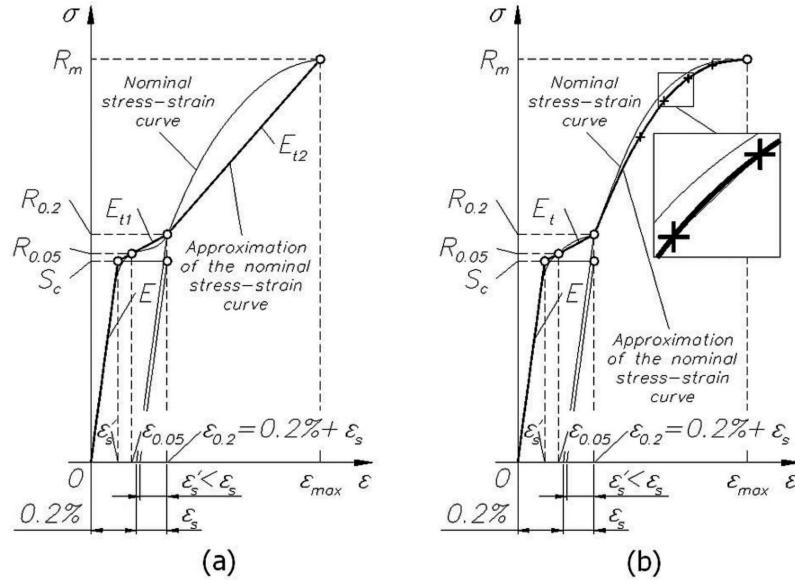
Fig. 9. Approximations of the real stress-strain curves $\sigma = f(\varepsilon)$ (displayed in the stretched scale)

of the first multi-linear approximation (Fig. 9a) were calculated from the set of equations

$$R_m - R_{0.2} - E_{t2} \left(\varepsilon_{\max} - \varepsilon_{0.2} \right) = 0,$$

$$R_{0.2} - R_{0.05} - E_{t1} \left(\varepsilon_{0.2} - \varepsilon_{0.05} \right) = 0, \tag{3}$$

$$R_{0.05} - E \varepsilon_s' - E_{t1} \left(\varepsilon_{0.05} - \varepsilon_s' \right) = 0,$$

$$S_c - E \varepsilon_s' = 0,$$

and are gathered in Table 3. In the second approximation (Fig. 9b), parabolic modeling was suggested beyond the yield limit. The parabola containing the point of coordinates $\varepsilon_{0.2}$, $R_{0.2}$ and reaching the maximum value at the point $\varepsilon_{\max}$, R_m was applied to describe the tensile behaviour of the material. For the numerical calculations, the parabola was replaced by several (twenty) segments of different slope but of equal length in the orthogonal projection at the ε axis. Such approximation enables direct introduction of the nonlinear material properties in the software module ANSYS$^{\circledR}$ which was used in the paper. Both approximations are conservative beyond the yield limit, although the second one is more precise. The similar approximation was proposed for the material used for the seats. However, the plastic deformations were present in the softer part of the junction, namely in the gasket only.

Moreover, it was assumed that the relationship between the equivalent stress σ_{eq} and equivalent strain ε_{eq} under complex stress states $\sigma_{eq} = f(\varepsilon_{eq})$ is

<div align="right">Table 3.</div>

<div align="center">Parameters of the first approximation of the stress-strain curves</div>

	Steel	S_c [MPa]	ε'_s [%]	ε_s [%]	E_{t1} [MPa]	E_{t2} [MPa]
Gasket	25CrMo4(N)	251.35	0.1248	0.159	3854.02	1756.37
Seat	42CrMo4(T)	808.26	0.3916	0.511	1329.88	1310.63

the same as the stress-strain relationship under uniaxial tensile loading $\sigma = $ $= f(\varepsilon)$. The stress intensity is derived from the von Mises yield criterion and the strain intensity is defined as [12]

$$\varepsilon_{eq} = \frac{2}{\sqrt{3}} \sqrt{\left(\varepsilon_z - \varepsilon_\varphi\right)^2 + \left(\varepsilon_\varphi - \varepsilon_x\right)^2 + \left(\varepsilon_x - \varepsilon_z\right)^2}, \qquad (4)$$

where ε_z, ε_φ and ε_x are the principal strains at a certain point of the cross-section.

The friction in contact zones was included in the proposed finite element model with the coefficient of friction assumed $\mu = 0.25$ [13].

5. Simplified analytical solution

5.1. The gasket

The waviness of the gasket working surface is small. The maximum relative difference of the thickness for the considered gaskets is less than 27.5%. For the continuous changes in thickness the gasket may be replaced by a cylindrical shell of a constant thickness t and a mean radius r, where t is defined as an arithmetic average of the two extreme values of the gasket thickness. The analytical investigations of the gasket were then based on a simple shell model of length $2l$ simply supported around the circumference at a contact with the seat. The spacing of the supports is $2h$ (Fig. 10). It is assumed that, except for a small region in the vicinity of supports, the shell is purely elastic.

The applied approach and permissible simplifications depend in the shell theory on the geometric proportions of the element. Following the estimation presented in [12, 14] for $0.05 < t/r < 0.1667$ and $2l < 2.4 \sqrt{(tr)}$ the shell is considered as "short" and of "mean thickness". This is the case, and the gasket must be solved on the basis of the bending shell theory and some terms in the differential equation of deflection could not be neglected.

Several computational models of the wave-ring gasket were created and investigated in [7] with the aim of selecting the simplest and most effective
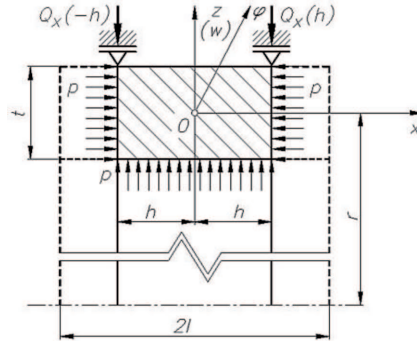
Fig. 10. Simplified computational model of the wave-ring gasket

one but sufficiently precise, which could be applied in the engineering approach. The analytical calculations verified by FEM modeling lead to the conclusion that the influence of external parts of the gasket outside of the supports (broken line in Fig. 10) is negligible. The relative difference in maximum equivalent stress σ_{eq} at the inside surface of the gasket is for this simplified model less than 2% with respect to the complete shell model with attached external segments. The results of the analysis confirm that the shell model of constant thickness simply supported at both ends at the inner surface of the seat in the cross-sections of coordinates $x = -h$ and $x = h$ is appropriate to describe the wave-ring gasket and leads to the good agreement with FEM modeling. At the assembly conditions the shell is loaded by shear forces at the supports only. At the service conditions the shell is additionally loaded by an operating pressure p acting at the inner cylindrical surface and at the edge plain surfaces. The seat must be considered as a thick-walled cylinder loaded by shear forces and by the internal pressure p.

Under the assumptions as for the cylindrical axisymmetrical shell of mean thickness t, mean radius r and small radial deflections w with respect to the thickness t, the differential equation of deflection for $p = 0$ (in the gaskets installation state) takes the form [12, 15, 16]

$$\frac{d^4w}{dx^4} + \beta^4 w = 0, \tag{5}$$

where $\beta = \sqrt[4]{12(1 - \nu^2)/r^2 t^2}$. The solution of equation (5) may be written as

$$w(x) = C_1 \cosh\left(\frac{\beta}{\sqrt{2}}x\right)\cos\left(\frac{\beta}{\sqrt{2}}x\right) + C_2 \sinh\left(\frac{\beta}{\sqrt{2}}x\right)\sin\left(\frac{\beta}{\sqrt{2}}x\right). \tag{6}$$

The constants of integration can be determined from the boundary conditions as for the simply supported shell, namely $w(h) = w_h$ and $M_x(h) = 0$

$$C_1 = \frac{c_1 c_3}{c_1^2 c_3^2 + c_2^2 c_4^2} w_h, \quad C_2 = \frac{c_2 c_4}{c_1^2 c_3^2 + c_2^2 c_4^2} w_h, \tag{7}$$

where the following substitutions are introduced

$$c_1 = \cosh\left(\frac{\beta}{\sqrt{2}}h\right), \quad c_2 = \sinh\left(\frac{\beta}{\sqrt{2}}h\right), \quad c_3 = \cos\left(\frac{\beta}{\sqrt{2}}h\right), \quad c_4 = \sin\left(\frac{\beta}{\sqrt{2}}h\right),$$

and w_h stands for the displacement of the support (the seat) caused by the interference Δ.

For the generalized Hooke's law in the case of two-dimensional stress state, the circumferential ε_φ and axial ε_x strains take the form

$$\varepsilon_\varphi = \frac{1}{E}\left(\sigma_\varphi - \nu\sigma_x\right), \quad \varepsilon_x = \frac{1}{E}\left(\sigma_x - \nu\sigma_\varphi\right), \tag{8}$$

where E and ν stand for the Young's modulus and Poisson's ratio, respectively. The stress may be determined from the equations

$$\sigma_\varphi = \frac{N_\varphi}{t} + \frac{12M_\varphi}{t^3}z, \quad \sigma_x = \frac{12M_x}{t^3}z, \tag{9}$$

where the internal cross-sectional forces and bending moments are expressed as

$$N_\varphi = \frac{Et}{r}w, \quad M_\varphi = K\nu\frac{d^2w}{dx^2}, \quad M_x = K\frac{d^2w}{dx^2}, \tag{10}$$

and the bending stiffness is $K = Et^3/12(1-\nu^2)$. The strains were measured at the inner cylindrical surface of the gasket so in equations (9) $z = -t/2$ must be taken at the inside of the gasket. The maximum equivalent von Mises stress σ_{eq} occurs at this surface and equals

$$\sigma_{eq} = \sqrt{\sigma_z^2 + \sigma_\varphi^2 + \sigma_x^2 - \sigma_z\sigma_\varphi - \sigma_\varphi\sigma_x - \sigma_x\sigma_z} \tag{11}$$

where under assembly conditions ($p = 0$) $\sigma_z = 0$.

5.2. The seat

The sectional seats 4 used in the test stand had relatively small thickness ratio (Fig. 3) with respect to engineering applications, in which the seats are executed directly in thick vessel walls. Moreover, the normal running fit (H/f) was applied at their outer diameter. The resultant displacement w_h (negative) at the support after assembly is then different from the designed radial interference Δ. As both elements are approximately of the same length (height), the resultant displacement w_h was finally determined basing on the thick-walled cylinders theory applied to the shell model and the seat, respectively [17]

$$|w_h| = \frac{\Delta}{2}\frac{\kappa_2^2 - 1}{\kappa^2 - 1}\left[\kappa_1^2(1-\nu) + 1 + \nu\right], \tag{12}$$

where $\kappa_1 = (2r + t)/(2r - t)$ is the ratio between the outer and inner radii of the shell, κ_2 is the ratio between the outer and inner radii of the seat and κ stands for the thickness ratio of the entire unit. The pressure at the contact surface of the cylinders corresponding to the interference Δ is

$$q = \frac{E\Delta}{2r + t} \frac{\left(\kappa_1^2 - 1\right)\left(\kappa_2^2 - 1\right)}{\kappa^2 - 1} \tag{13}$$

and may be additionally used to estimate the shear force at the support

$$Q_x = \frac{1}{2} 2ql. \tag{14}$$

5.3. The wavy working surface

Special attention must be paid to the interaction conditions between the wavy working surface of the gasket and the cylindrical surface of the seat (Fig. 2). Initial assembly interference Δ is usually of great value (more than 0.5‰), and the difference in mechanical properties of the materials may cause the plastic process in the gasket. The Hertz theory was applied to calculate the stress distribution in the contact region and to the initial estimation of the width of this region. The radius $\varnothing A/2$ of the seat is usually much greater than the radius R_1 of curvature (in the considered example more than four times). The Hertz approach for an elastic cylinder of radius R_1 being in contact with a rigid plane seems to be appropriate in this case, which leads to the parabolic elastic distribution $q(x)$ of stress with the maximum value [18]

$$q_{\max} = 0.418 \sqrt{\frac{Q_x(h)E}{R_1}}, \tag{15}$$

and to the width of the contact region

$$e = 3.045 \sqrt{\frac{R_1 Q_x(h)}{E}}, \tag{16}$$

where $Q_x(x)$ stands for the continuous uniformly distributed load acting at the cross section of the contact and may be calculated as a reaction at the support $Q_x(x) = dM_x(x)/dx$ (Fig. 10).

Elastic distribution of the contact stress $q(x)$ is depicted in Fig. 11a. In these regions, where the stress $q(x)$ calculated from the initial elastic Hertz distribution is considerably beyond the yield limit $R_{0.2}$ of the gasket material, the plastic process must appear. As a result, a redistribution of the initial elastic stress $q(x)$ must occur and finally a resultant stress distribution $q_{pl}(x)$ must appear which allows for the plastic deformations (Fig. 11b).
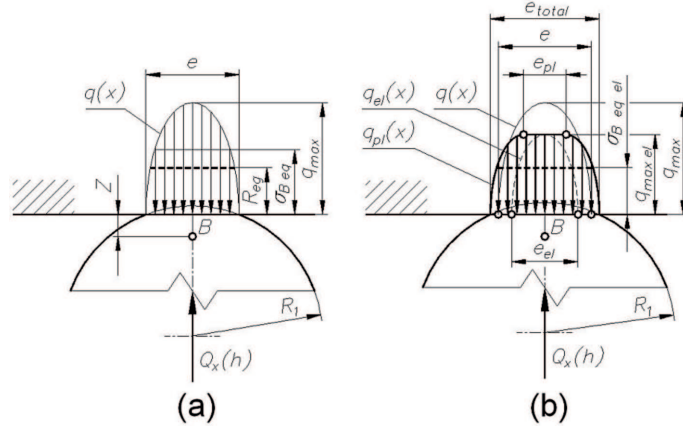
Fig. 11. Distribution of stress at the contact region of the gasket and the seat: (a) – elastic (parabolic) with respect to the Hertz theory; (b) – changed (partially-linear) with respect to plastic deformation

The first and rough estimation of the width e of the contact region is carried out under the assumption that the gasket material satisfies pure elastic-plastic stress-strain relationship and the seat material is perfectly rigid. Moreover, it is assumed that the plastic deformations begin when the gasket is subjected to the load $Q_x(h)$ which produces the stress $q_{\max} = R_{0.2}$. Under the load which produces the stress $q_{\max}$ which is n − times greater than the yield limit $R_{0.2}$ ($q_{\max} = nR_{0.2}$), the elastic parabolic distribution $q_{el}(x)$ corresponding to the load $Q_{x\,el}(h) \leq Q_x(h)$ in the contact surface will exist, for which the maximum stress equals $q_{\max\,el}$. The width of the contact region satisfying the above elastic Hertz distribution $q_{el}(x)$ with respect to the distribution $q(x)$ is

$$e_{el} = \frac{1}{n}e. \tag{17}$$

The surplus shear load $\Delta Q_x(h) = Q_x(h) - Q_{x\,el}(h)$ produces the plastic process which leads under the applied assumptions to the plastic deformation. A new partially-linear stress distribution $q_{pl}(x)$ is introduced to describe the problem (Fig. 11b). The width of the additional plastic zone is determined from the condition that the entire shear force $Q_x(h)$ does not change

$$e_{pl} = \frac{2}{3}\left(n - \frac{1}{n}\right)e. \tag{18}$$

The total width of the contact region may be then calculated as a sum of the elastic contact e_{el} (17) and plastic contact e_{pl} (18)

$$e_{total} = \left(2n + \frac{1}{n}\right)\frac{e}{3}. \tag{19}$$

Another approximate approach follows the Bielaev's theory, in which the maximum equivalent stress σ_{Beq} is expected at the point B placed at the distance $Z = 0.349e$ under the contact surface (Fig. 11a), and in this case equals [18]

$$\sigma_{Beq} = 0.251\sqrt{\frac{Q_x(h)E}{R_1}}. \tag{20}$$

Due to the Bielaev's theory, the plastic process in the gasket material may occur if $\sigma_{Beq} \geq R_{0.2}$. Comparison of the equivalent Bielaev's stress (20) and the maximum Hertz stress (15) leads to the conclusion that $q_{max}/\sigma_{Beq} = 1.665$, which means that the plastic process appears in the contact region only if the maximum stress $q_{max} \geq 1.665R_{0.2}$.

A similar as above distribution $q_{pl}(x)$ is introduced under additional assumption that the plastic process initiated at the Bielaev's point B expand to the contact surface. Assuming that the cylinder is subjected to the load $Q_x(h)$ which causes that the Bielaev's equivalent stress is n_B – times greater than the yield limit $R_{0.2}$ ($\sigma_{Beq} = n_B R_{0.2}$), in the contact surface may only exist elastic parabolic distribution $q_{el}(x)$ corresponding to the load $Q_{xel}(h) \leq Q_x(h)$, for which the maximum stress equals $q_{max\,el}$ and $\sigma_{Beq\,el} = R_{0.2}$ (Fig. 11b). The total width of the contact region may be determined from equation (19), however, in this case the factor n_B is much less than n.

The analytical approach – in particular the first estimation of the width e of the contact region – based on the assumption of constant pressure along a part of the contact zone where the plastic deformations are expected, is rough and questionable. However, this approach leads to the results which are closer to more precise numerical results and to the test results than the second analytical approach based on the Bielaev's theory. The above simple approach can be recommended for the preliminary calculations of the closures. The suggested simplified distribution of the contact stress $q_{pl}(x)$ must be treated as a highly approximate one. The assumption of the pure elastic-plastic stress-strain curve of the gasket material leads to the overestimation of the total width of the contact region. On the other hand, the width of the contact region seems to be underestimated because it is assumed that the stress $q_{max\,el} = 1.665R_{0.2}$ is acting along the entire length e_{pl} in the proposed model.

6. Comparison of the test results with FEM simulation and analytical approach

The circumferential and axial strains were measured in the test at the inner cylindrical surface of the gaskets. For this reason, they were directly compared with the strains obtained in FEM method (Section 4) and with

those calculated using simplified analytical approach – equation (8). The gaskets and the seats were executed with the specified tolerances so the resultant radial interference Δ may change from the minimum value Δ_{min} to the maximum value Δ_{max}. The FEM calculations and analytical investigations were carried out for the nominal interference Δ_{nom} and for the limit interferences Δ_{min} and Δ_{max}.

The exemplary distributions of strains are depicted in Fig. 12 for the group 2 of gaskets where the results for both numerical methods FEM 1 and FEM 2 are presented. The wide dashed lines correspond to the FEM 1 approach where the interferences were arranged by means of the thermal method (sticking) while the solid lines correspond to the FEM 2 approach in which the assembly process was simulated by means of sliding of the seats with respect to the gasket. The narrow dashed lines present the results obtained using the analytical solution.

The influence of the friction coefficient on the FEM results is shown in Fig. 13, in which the calculations for the second numerical approach are carried out for several values of μ. The increase of μ results in the simultaneous increase of the equivalent stress σ_{eq} in the vicinity of the gasket midpoint and at the edge assembled in the first order and in the decrease of σ_{eq} at the edge assembled in the second order. However, the changes in stress are negligible: the increase of the friction coefficient from $\mu = 0.25$ to $\mu = 0.50$ produces the difference in stress less than 4% at the midpoint and less than 10% at the edge for $x = 35$ mm. For this reason the friction coefficient $\mu = 0.25$ was accepted in the numerical calculations which is in accordance with the experimental tests carried out for certain deformable joints [13]. Moreover, this value of μ is additionally confirmed by comparison of the assembly forces recorded in the test and the forces calculated for the results obtained in the FEM simulation.

Even less influence on the equivalent stress distributions has the approximation of the stress-strain curves therefore in both numerical methods FEM 1 and FEM 2 the first simple (multi-linear) approximations of the real stress-strain curves were introduced into the numerical procedure.

It should be noted that the test results demonstrate rather poor central symmetry. This disturbance appears also in the strain distributions corresponding to the FEM 2 method (Fig. 12 – solid lines) and is caused by different assembly conditions for both sectional seats. Another reason is that different effective interferences (within the limit interferences) may exist for the same gasket and both sectional seats. The asymmetry of test results is additionally confirmed by different assembly and disassembly forces recorded in the test. The greater values of strains correspond to greater values of forces at the same side of the gasket.
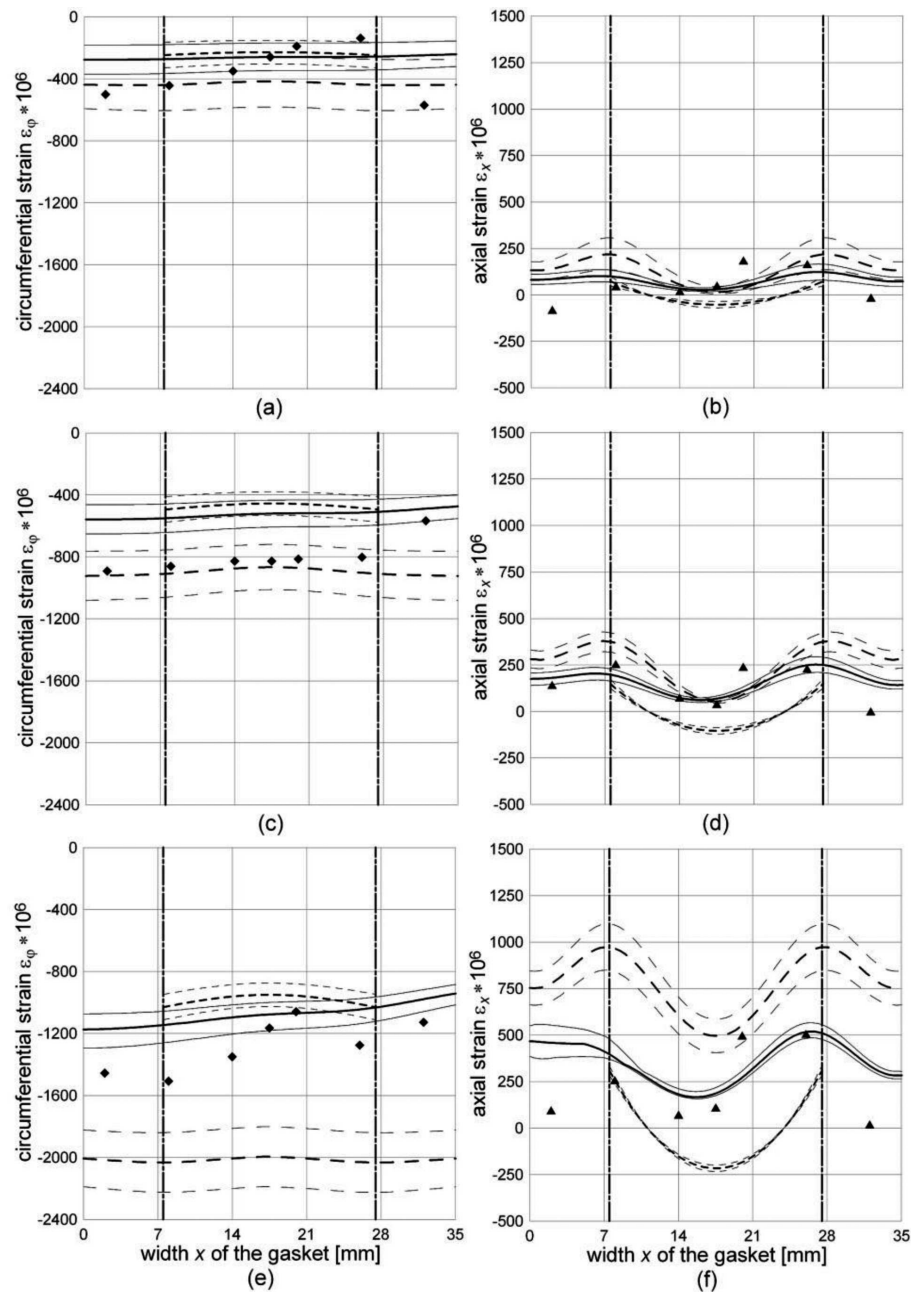
Fig. 12. Comparison of strains: (a), (c), (e) – circumferential ε_φ; (b), (d), (f) – axial ε_x for sets: (a), (b) – 2A; (c), (d) – 2B; (e), (f) – 2C. Labels: ♦, ▲ – test results; wide dashed lines – FEM 1 results, solid lines – FEM 2 results, narrow dashed lines – analytical results; bold lines – results for the nominal interference, fine lines – results for the limit interferences
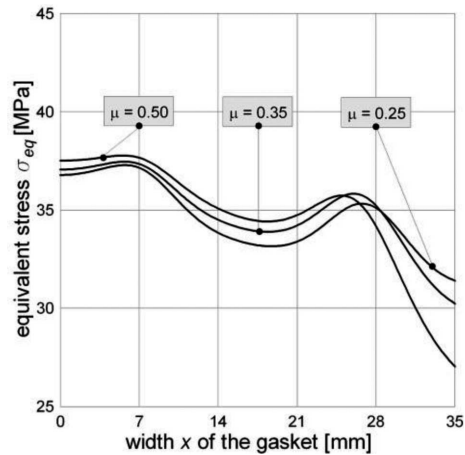
Fig. 13. Comparison of equivalent stress σ_{eq} for set 2A ($\Delta_{nom} = 0.48$‰) and several values of the friction coefficient μ for the minimun interference Δ_{min}

Investigation of strain distributions presented in Fig. 12 leads to the conclusion that the change of loading of the gaskets and application of the numerical model FEM 2 similar to real test conditions cause that the numerical results are closer to the test results. The same tendency may be noticed in the distributions of the equivalent stresses σ_{eq} at the inner surface of the gaskets presented in Fig. 14.
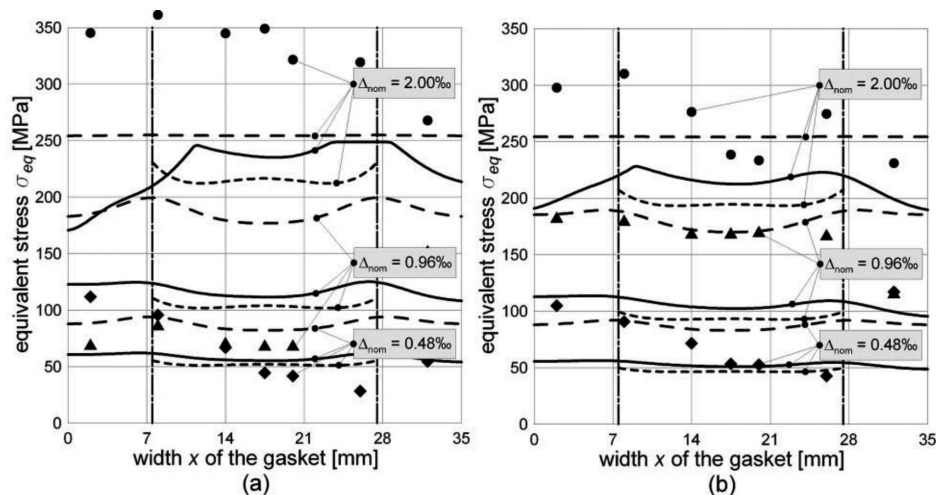

Fig. 14. Comparison of equivalent stress σ_{eq} at the inner surface of the gaskets: (a) – for group 1 and (b) – for group 2. Labels: ♦, ▲, • – test results for the nominal interferences 0.48‰, 0.96‰, 2.00‰, respectively. Wide dashed lines – FEM 1 results for the nominal interference, solid lines – FEM 2 results for the nominal interference, narrow dashed lines – analytical results for the nominal interference

Most of the test results for the set 2A obtained for the small nominal radial interference 0.48‰ are placed inside the range received by FEM 2 method and the analytical approach – Fig. 12a, b. The greater interferences (0.96‰ and 2.0‰) result in respectively greater differences between FEM 1 and FEM 2 methods and analytical solutions whereas the test results are located between FEM 1 and analytical results. Investigation of experimental and theoretical strain distributions depicted in Fig. 12 leads to the conclusion that the FEM 1 method is overestimated, and analytical calculations are underestimated with respect to the experiment and that the difference increases with the increase of the initial interference fit. The results obtained using FEM 2 method are placed between FEM 1 method and analytical results.

The relation between the width of the contact zone and the applied interference fit is an important feature of the joint. In the gasket installation state, this relation depends also on the value of the yield limit of the gasket material. The width of the contact traces at the working surface of the gaskets calculated applying first strongly simplified approach (analytical 1 – Table 4) are similar to those obtained using the more precise FEM 2 approach for the specific material of the gasket. The results gathered in Table 4 present the obvious tendency as the increase of the interference causes simultaneous increase of the width of the contact region. The results arrived at by means of the Bielaev's theory are lower than the presented ones and the difference increases from about 25% for the nominal interference 0.48‰ to 35% for the nominal interference 2.0‰. The width of contact traces at the wave surfaces of gaskets measured after disassembly the closures differs significantly for the same interference and for the same trace. The relative difference increases with increasing of the interference and exceeds even 50%. The reason is that for greater interference fits the plastic process is engaged. However, the formulation of the relationship between the growth of plastic zone at the contact and the increasing of the interference values needs further analytical and numerical investigations supported by the experimental tests.

Table 4.

Comparison of the width of the contact traces

No. group	No. set	Δ_{nom} [‰]	Width of the contact trace e [mm]											
			Test			FEM 2			Analytical 1			Analytical 2 (Bielaev)		
			min	nom	max	min	nom	max	min	nom	max	min	nom	max
2	A	0.48	0.50	0.70	0.90	0.314	0.295	0.401	0.209	0.292	0.375	0.181	0.222	0.272
	B	0.96	1.10	1.15	1.20	0.464	0.546	0.619	0.458	0.540	0.623	0.322	0.371	0.421
	C	2.00	0.95	2.05	3.15	0.896	0.954	1.009	0.997	1.079	1.162	0.645	0.695	0.745

The working surfaces of the gaskets from group 2 after disassembly are shown in Fig. 15. It appears that the interference of $\Delta = 2.0\%_0$ caused visible failures of the gaskets.
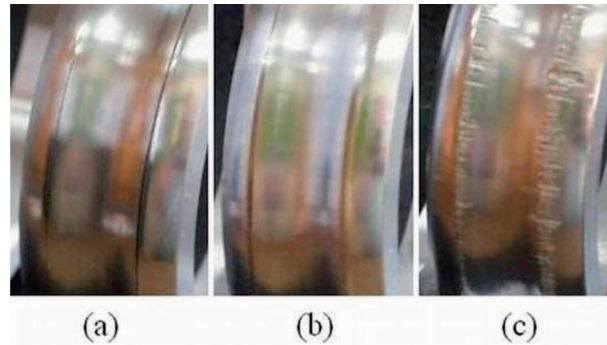

Fig. 15. Group 2 after disassembly. Interferences Δ_{nom}: (a) – $0.48\%_0$; (b) – $0.96\%_0$; (c) – $2.00\%_0$. Note the contact traces

7. Final remarks

As a result of an experiment, the distributions of circumferential and axial strains at the inner surface of the wave-ring gasket were obtained. The gaskets were examined under assembly conditions. During the test, the gaskets were pressed into the seats and no operating pressure was applied to the closure. The experimental results were verified by FEM calculations. Additionally, the simplified analytical approach based on the shell theory was applied to verify the test results. The comparison of experimental and theoretical results reveals that FEM modeling leads to the overestimation, while analytical calculations are underestimated with respect to the test.

The analytical computational model of the closure may be convenient to proceed an initial analysis. A large number of simple calculations can be carry out for different geometry of the gasket, different material properties and assembly requirements. The final parameters of the closure may be then determined in the detailed FEM verification.

The leak tightness of the joint depends in particular on the applied initial assembly interference. Visual inspection of the gaskets after the disassembly indicates that the designed interference must be less than $2.0\%_0$ for the unchanged another parameters of the investigated closure. Too much radial interference fit with respect to the yield limit of the gasket material was probably the main reason of the serious damage of the working surface. In this case, the applied interference fit together with the large value of the friction coefficient lead during the assembly (and disassembly) operation under load in the absence of adequate lubricant to the adhesive wear [19]. The original

adhesion theory postulated that all asperity contacts would result in yielding and adhesion due to the high stresses present. When clean surfaces are pressed against one another under load, some of the asperities in contact will tend to adhere to one another due to the attractive forces between the surface atoms of the two materials. As sliding between the surfaces is introduced, these adhesions are broken, either along the original interface or along a new plane through the material of the asperity peak. In the latter case, a piece of one part is transferred to another part, causing surface disruption and damage. Sometimes, a particle of one material will be broken free and become debris in the interface, which can then scratch the surface and plough furrows in both parts. This damage is called scoring or scuffing of the surface.

The experimental investigations point out that the manufacturing process of wave-ring gaskets must ensure the high dimensional accuracy, in particular with respect to the working surface. Moreover, the gasket installation and replacement operations should be carried out with extreme precision. The attention must be paid to the exact alignment of the gasket with respect to the seat, above all in closures with great diameter. The inaccurate mounting process results in scaring of the wave surface of the gasket.

REFERENCES

[1] Freeman A.R.: Gaskets for high-pressure vessels. In: Pressure Vessel and Piping Design. Collected Papers 1927-1959, 1960, pp. 165-168.

[2] Realization of technical documentation of the reactor 41/42 V-7 for the polyethylene installation. Report TPP-5 Cracow University of Technology, 2000.

[3] Ryś J.: An analysis of high-pressure connections with wave-ring gasket, Proc. XXI Symposium on Machine Design, 2003, Vol. II, pp. 183-188.

[4] Ryś J., Trojnacki A., Betleja T.: Theoretical analysis of metal wave-ring gasket for high-pressure joints, Proc. Xth Int. Conf. Seals and Sealing Technology in Machines and Devices, 2004, pp. 54-62.

[5] Szybiński B., Trojnacki A.: Experimental verification of stress-strain analysis of metal wave-ring gasket. Mechanical Review, 2011, Vol. 7-8'11, pp. 50-57.

[6] Trojnacki A.: Druckstandfestigkeit und Betriebseigenschaften von Doppelwellendichtungen. Chemie Ingenieur Technik, 2011, Vol. 83, No. 3, pp. 377-385.

[7] Ryś J., Szybiński B., Trojnacki A.: Computational model of metal high-pressure wave-ring gasket. Technical Transactions, 2006, z. 11-M/2006, pp. 63-87.

[8] ANSYS. Release 8.0. Swanson, Analysis System Inc., 2003.

[9] Wriggers P.: Computational contact mechanics. West Sussex, John Wiley&Sons, Ltd, 2002.

[10] Krasiński M., Szybiński B.: Numerical analysis of contact problems in high pressure sealing, Proc. XXII Symposium on Machine Design, 2005, Vol. III, pp. 227-232.

[11] Stein E.: Error-controlled adaptive finite elements in solid mechanics. West Sussex, John Wiley&Sons, Ltd, 2003.

[12] Życzkowski M. (Ed.): Technical Mechanics. Vol. IX, Strength of structural elements. Warszawa, PWN, 1988.

[13] Krukowski A., Tutaj J.: Deformable joints. Warszawa, PWN, 1987.

[14] Woźniak C. (Ed.): Technical Mechanics. Vol. VIII, Mechanics of elastic plates and shells. Warszawa, PWN, 2001.

[15] Kozłowski T.: Theory of plasticity. Warszawa, Arkady, 1968.

[16] Timoshenko S., Woinowsky-Krieger S.: Theory of plates and shells. Warszawa, Arkady, 1962.

[17] Walczak J.: Strength of materials and elements of elasticity and plasticity. Warszawa, PWN, 1973.

[18] Bijak-Żochowski M. (Ed.): Strength of structures, Vol. 2. Warszawa, Editorial Board of Warsaw University of Technology, 2004.

[19] Norton R.L.: Machine design. An integrated approach. New Jersey, Pearson Education LTD, 2006.

Analityczne i numeryczne obliczenia metalowej wysokociśnieniowej uszczelki typu B i porównanie z wynikami badań doświadczalnych

S t r e s z c z e n i e

W pracy przedstawiono wyniki badań doświadczalnych zestawu metalowych wysokociśnieniowych uszczelek typu „B", różniących się grubością i wciskiem montażowym. Badania wykonano w warunkach montażowych po wprowadzeniu uszczelek w gniazda, bez obciążenia połączenia ciśnieniem roboczym. Na wewnętrznej, cylindrycznej powierzchni uszczelek mierzono odkształcenia obwodowe i osiowe przy użyciu tensometrów oporowych. Po odciążeniu i demontażu zmierzono szerokość strefy kontaktu plastycznie odkształconej powierzchni roboczej uszczelki. Zostały również wykonane badania materiałowe uszczelek oraz gniazd. Przeprowadzono numeryczną weryfikację wyników pomiarów za pomocą obliczeń MES, w których uwzględniono nieliniowe własności materiałów złącza, efekty kontaktowe oraz tarcie na powierzchni kontaktu. Dodatkowo porównano wyniki pomiarów z obliczeniami analitycznymi, otrzymanymi w oparciu o uproszczony powłokowy model uszczelki.